LARGE EDDY SIMULATION AND MEASUREMENTS IN A TURBULENT ROTOR-STATOR FLOW

Séverac Éric, Poncet Sébastien, Serre Éric

MSNM-GP UMR6181 CNRS
IMT La Jetée, Technopôle de Château-Gombert, 38 rue F. Joliot Curie, 13451 Marseille, France
severac / poncet / serre1@l3m.univ-mrs.fr

Chauve Marie-Pierre
IRPHE UMR6594 CNRS
Technopôle de Château-Gombert, 49 rue F. Joliot Curie, BP 146, 13451 Marseille, France
chauve@irphe.univ-mrs.fr

ABSTRACT

Comparisons between large eddy simulation (LES) and velocity measurements have been performed for a turbulent flow in a real shrouded rotor-stator configuration. The LES model is based on Spectral Vanishing Viscosity (SVV). The key particularity of this model is that the SVV is active only at the short length scales, a feature which is required to accurately capture the complexity of the flow. Thus, numerical results are shown to compare very favourably with experimental measurements at rotational Reynolds numbers $Re = \Omega.b^2/\nu = 10^6$ in an annular cavity of radius ratio $s(= a/b) = 0.286$ and of aspect ratio $G = (b-a)/h = 5$, where a and b are respectively the inner and outer radii of the rotating disk and h is the inter-disk spacing. The spectral vanishing viscosity, first introduced by E. Tadmor for the inviscid Bürgers equation [SIAM J. Numer. Anal. 26, 30 (1989)], is incorporated into the cylindrical Navier-Stokes equations written in velocity pressure formulation. The second-order operator involved by the SVV-method is implemented in a Chebyshev-collocation Fourier-Galerkin pseudo-spectral code. As far as the authors are aware, LES of fully turbulent flow in an actual shrouded rotor-stator cavity have not been performed before.
Keywords: rotor-stator flow, large eddy simulation, spectral vanishing viscosity technique, LDV.

INTRODUCTION

There have been numerous numerical simulations and experimental studies of flow between rotating and stationary discs, with a stationary shroud and through-flow (a "rotor-stator cavity") (see references in Serre et al. ,2001; Poncet et al. ,2005; Randriamampianina and Poncet ,2006). The flow has significant industrial applications, such as internal gas-turbine flows and computer hard disks, and the geometry is relatively simple. A characteristic feature of such flows is the coexistence of adjacent coupled flow regions that are radically different in terms of the flow properties (Serre et al. , 2004).

In the laminar regime, Batchelor (see Fig. 1) solved the problem relative to the stationary axi-symmetric flow between two infinite disks. He specified the formation of a non-viscous core in solid body rotation, confined be-tween two boundary layers. In contrast, Stewartson claimed that the tangential velocity of the fluid can be zero everywhere apart from the Ekman layer on the rotor. This controversy ended when Mellor discovered numerically the existence of a multiple class of solutions showing that both Batchelor and Stewartson flow structures can be found from the similarity solutions.

Daily and Nece (1960) have carried out an exhaustive theoretical and experimental study of sealed rotor-stator flows. They pointed out the existence of four flow regimes depending upon combination of the rotation speed and the inter-disk spacing. These correspond respectively to two laminar regimes (I and II) and two turbulent regimes (III and IV), each characterized by either merged (I and III) or separated (II and IV) boundary layers. In the latter case, the flow is of Batchelor type with two boundary layers separated by a central rotating core. They provided also an estimated value for the local Reynolds number at which turbulence originates with separated boundary layers, $Re_r = \Omega r^2/\nu = 1.5 \times 10^5$ (r is the radial location) for aspect ratios $G(= (b-a)/h) < 25$. However, experiments have revealed that transition to turbulence can appear at a lower value of Re_r within the Bödewadt layer on the stator, even though the flow remains laminar in the Ekman layer along the rotor. From detailed measurements, Itoh et al. (1995) reported a turbulent regime occurring earlier along the stator side at $Re_r = 8 \times 10^3$, while along the rotor side, turbulent flow develops later for $3.6 \times 10^5 < Re_r < 6.4 \times 10^5$ for $G = 12.5$. This is in agreement with the experiment of Cheah, for which the flow along the rotor side is turbulent for $Re_r = 4 \times 10^5$ ($G = 7.87$). Differences in turbulence characteristics between the rotor and stator sides have also been observed and attributed to the effects of the radial convective transport of turbulence.

As a consequence, only a few investigations of turbulent rotating disks flows have been done, using Large Eddy Simulation (LES) based on filtered Navier-Stokes equations. To our knowledge, only two studies performed by Wu and Squires (2000) and Lygren and Andersson (2001) provided useful results. Wu and Squires performed LES of the three-dimensional turbulent boundary layer over a free rotating disk at $Re = 6.5 \times 10^5$ and in an otherwise quiescent incompressible fluid using periodic boundary conditions both in the radial and tangential directions. The authors used three different dynamical models to model the sub-grid scale stress arising from the filtering operation: the eddy viscosity model of Germano, the mixed model of Zang and the

mixed model of Vreman. Their results have offered new evidence to support the observations of Littell and Eaton (1994) that streamwise vortices with the same sign as the mean streamwise velocity are mostly responsible for strong sweep events, while streamwise vortices with opposite sign to the mean streamwise velocity promote strong ejections. Using the same assumptions as in their DNS investigation, Lygren and Andersson (2004) performed LES of a rotor-stator flow for Reynolds numbers ranging from $Re = 4 \times 10^5$ to $Re = 1.6 \times 10^6$. Using both the dynamic subgrid-scale model proposed by Lilly and the mixed dynamic model due to Vreman, Lygren and Andersson concluded that the best overall results where obtained with the second model. These authors performed LES for five different aspect ratios, ranging from the wide-gap cavity to the narrowgap one. As for Wu and Squires, their LES study supported the view of Littell and Eaton that the mean flow three-dimensionality affects the near wall vortices and their ability to generate shear-stresses.

Following this reasoning, a numerical method is proposed here to provide accurate solutions to these flows in turbulent regimes based on a highly accurate spectral method that uses expansions in Chebychev polynomials and Fourier series to approximate the solution of the Navier-Stokes equations (NSE) in the non-homogeneous and tangential directions, respectively. Finally, turbulent regimes are investigated here in an annular rotor-stator cavity, using experimental measurements as well as Large-Eddy Simulation (LES). At our knowledge, there has been no efficient investigation of turbulent rotor-stator flows within a closed interdisk cavity using LES. The mean flow is mainly governed by three control parameters: the aspect ratio of the cavity $G(= (b-a)/h) = 5$, the rotational Reynolds number $Re = \Omega.b^2/\nu$ based on the outer radius b of the rotating disk and the radius ratio $s(= a/b) = 0.286$. In this work, LES and experimental measurements have been used to characterize statistical properties of turbulent rotor-stator flows at Reynolds numbers $Re = 10^6$.

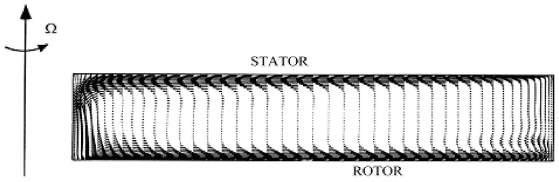

Figure 1: Laminar Batchelor's flow (DNS result). Instantaneous velocity field in the meridian plane $(r, \theta/4, z)$ at $Re = 10000$.

GEOMETRY

The cavity is composed by two smooth parallel disks of radius $b = 140mm$, one rotating at a uniform angular velocity Ω (rotor), one being at rest (stator). The disks are delimited by an inner cylinder (the hub) of radius $a = 40mm$ attached to the rotor and by an outer stationary casing (the shroud) slightly larger than the rotor. The cavity is filled with water maintained at a constant working temperature 20^oC.

INSTRUMENTATION AND MEASUREMENTS

The measurements are performed using a two component laser Doppler anemometer (LDA). The LDA technique is used to measure from above the stator the mean radial V_r and tangential V_θ velocities as well as the associated three Reynolds stress tensor components in a vertical plane (r, z). This method is based on the accurate measurement of the Doppler shift of laser light scattered by small particles (Optimage PIV Seeding Powder, $30\mu m$) carried along with the fluid. Its main qualities are its non intrusive nature and its robustness. About 5000 validated data are necessary to obtain the statistical convergence of the measurements. It can be noticed that, for small values of the interdisk space h, the size of the probe volume ($0.81mm$ in the axial direction) is not small compared to the boundary layer thicknesses and to the parameter h.

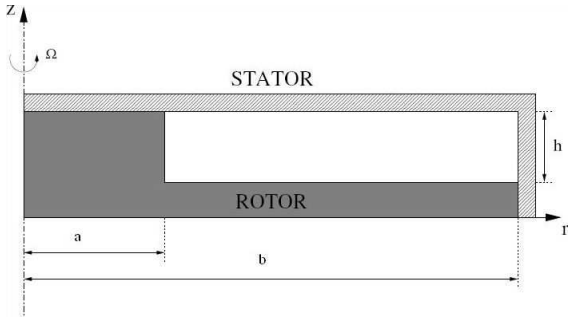

Figure 2: Details of the cavity and the geometric parameters.

NUMERICAL MODELLING

The incompressible fluid motion is governed by the three-dimensional Navier-Stokes equations written in primitive variables (see below).

$$\begin{cases} \frac{\partial \overrightarrow{V}}{\partial t} + div(\overrightarrow{V} \otimes \overrightarrow{V}) = -\overrightarrow{grad}p + \frac{1}{Re}\overrightarrow{\Delta V} & \text{in } D \\ div\,\overrightarrow{V} = 0 & \text{in } \overline{D} \\ \overrightarrow{V} = \overrightarrow{W} & \text{on } \Gamma \end{cases} \quad (1)$$

where t is the time, $\overrightarrow{V}$ is the velocity of components (u,v,w) in the radial, tangential, and vertical direction respectively, for cylindrical coordinates $(r,\ \theta,\ z)$, p is the pressure; and Γ denotes ∂D, and $\overline{D}$ denotes $D \cup \partial D$. This equation is completed by initial conditions for the velocity:

$$\begin{cases} \overrightarrow{V}(t=0) = \overrightarrow{V_0} & \text{in } \overline{D} \\ \text{with } div\overrightarrow{V_0} = 0 & \text{in } \overline{D} \end{cases} \quad (2)$$

The temporal discretization adopted in this work is a projection scheme, based on backwards differencing in time. The projection scheme requires the solution of a pressure Poisson equation to (approximately) maintain solenoidality of the velocity (see Raspo et al. 2002). The specificity of our algorithm lies in the computation at each time step of a pressure predictor (through this pressure Poisson equation is augmented with a pressure Neumann boundary condition obtained with a projection of the momentum equation on the normal direction to the domain), which allows the correct temporal evolution of the normal pressure-gradient at the boundaries during the time integration. The equations are discretized in time using a second-order semi-implicit scheme which combines a second order backward differential Euler scheme for the unsteady term, an implicit scheme for the diffusive term, and an explicit Adams-Bashforth extrapolation for the non-linear convective terms. Its good stability properties for an advection-diffusion equation have been shown before by Raspo et al. (2002).

In the radial and axial directions, as boundary layers develop in the meridian plane, a collocation Chebychev approximation is used associated with Gauss-Lobatto collocation.

Then, for each Fourier mode, the solution $(\overrightarrow{V},\, p)$ is approximated by Chebyshev polynomials of degree at most equal to N_1 in the radial direction and to N_3 in the axial direction. On the other hand, a standard Fourier-Galerkin approximation is employed for the solution in the 2π-periodic direction. We note that $N_2/2$ is the cut off frequency of the Fourier series.

For the computation of the non-linear terms, a pseudo-spectral technique is used, specifically. The derivatives in each direction are calculated in the spectral space and the products are calculated in the physical space as presented in the book of Peyret. A FFT algorithm is used to connect the spectral and the physical spaces. On the other hand, the implicit diffusive term is evaluated through spectral differentiation matrices.

Finally, for each Fourier mode, a full diagonalization technique is used to solve a set of 2D uncoupled Helmholtz and Poisson problems obtained after splitting the Euler scheme to group the implicit part in the left hand side of the equations (see a detailed analysis in Serre et al. , 2001).

The LES is performed through a Spectral Vanishing Viscosity technique (SVV) (see Tadmor ,1989). A second viscosity term is incorporated in the Helmholtz equations of velocity prediction. It is build (see below) appropriately to be only active for high wave numbers of the numerical approximation not to affect the large scale of the flow and to stabilise the solution by increasing the dissipation where it is needed the most: near the cut off frequency.

There is no direct way to extend the SVV operator created by Tadmor to the 3D case. But following the investigations of Pasquetti et al. (2002), and Karamanos & Karniadakis (2000), we choose to define our SVV operator as follow:

$$\begin{cases} \widetilde{\Delta V_N} = div(grad(V_N) \times Q_N) \\ \text{with } Q_N = diag(Q^i_{N_i}) \end{cases} \tag{3}$$

where V_N denotes the approximation of the velocity vector $\overrightarrow{V}$; Q_N denotes the 3D SVV operator that is com-posed of three 1D SVV operators $Q^i_{N_i}$; $i = 1, 2, 3$ corresponding to the $(r,\, \theta,\, z)$ directions respectively. Moreover the 1D operators are only defined in spectral space as a C^∞ smooth function:

$$\begin{cases} \hat{Q}^i_{N_i}(\omega) = \begin{cases} 0 & 0 \le \omega \le \omega_{T_i} \\ \epsilon_{N_i} \times e^{-\left(\frac{\omega_{c_i}-\omega}{\omega_{T_i}-\omega}\right)^2} & \omega_{T_i} < \omega \le \omega_{c_i} \end{cases} \\ \epsilon_{N_i} = O(\frac{1}{N_i}) \\ \omega_{T_i} = O(\omega_{c_i}) \\ 0 \le \omega_{T_i} < \omega_{c_i} \end{cases} \tag{4}$$

where ϵ_{N_i} are the maximum of viscosity; ω_{T_i} and ω_{c_i} are the threshold after which the viscosity is applied and the highest frequency calculated in the direction i, respectively.

Because our SVV operator is fully linear, we can group it with the implicit part of our Helmotz equations (as long as the parameters aren't time dependent) to be diagonalized with the standard viscosity term. The resulting scheme can be globally written as follow:

Prediction step

$$\begin{cases} \Delta p^*_N = -div(AB_2(div(V_N \otimes V_N)) & \text{in D} \\ \overrightarrow{grad p^*_N} = \begin{cases} BDE_2(V_N) \\ -AB_2(div(V_N \otimes V_N)) \\ -\frac{1}{Re} rot(rot(AB_2(V_N))) \end{cases} & \text{on } \Gamma \end{cases} \tag{5}$$

$$\begin{cases} \frac{1}{Re}\Delta V^*_N + \widetilde{\Delta V^*_N} = \begin{cases} BDE_2(V_N) \\ +\overrightarrow{grad p^*_N} \\ +AB_2(div(V_N \otimes V_N) \end{cases} & \text{in D} \\ V^*_N = W_N & \text{on } \Gamma \end{cases} \tag{6}$$

Correction (projection) step

$$\begin{cases} \Delta \phi_N = div(V^*_N) & \text{in D} \\ \overrightarrow{grad}\phi_N = 0 & \text{on } \Gamma \end{cases} \tag{7}$$

$$\begin{cases} V^{n+1}_N = V^*_N - \overrightarrow{grad}\phi_N & \text{in } \overline{D} \\ p^{n+1}_N = p^*_N - \frac{2}{3\delta t}\overrightarrow{grad}\phi_N + \Delta\phi_N & \text{in } \overline{D} \end{cases} \tag{8}$$

where p^*_N is our pressure predictor that leads to an estimation of the velocity for the next time step V^*_N that may not be divergence free, hence the use of the projector ϕ_N to recover the final solution (V^{n+1}_N, p^{n+1}_N) of the next time step. $AB_2(\psi)$ and $BDE_2(\psi)$ denote the explicit second order Adams-Basforth extrapolation and the implicit second order backward Differential Euler scheme, respectively, of a given function ψ.

RESULTS

$Re = 4 \times 10^5$

The flow regime is transitional turbulent, characterized by a fully turbulent stationary disk layer and a transitional turbulent rotating disk layer at mid to large radius (see Fig. 3). SVV computation has been carried out on the grid $(N_1, N_2, N_3) = (121, 180, 65)$ with a time step $\delta t = 10^{-4}\Omega^{-1}$. The SVV parameters have been chosen equal to $(\epsilon_1, \epsilon_2, \epsilon_3) = (\frac{1}{2.N_1}, \frac{1}{N_2}, \frac{1}{2.N_3})$ and $(\omega_{T_1}, \omega_{T_2}, \omega_{T_3}) = (\sqrt{\omega_{c_1}}, \sqrt{\omega_{c_2}}, \sqrt{\omega_{c_3}})$. The statistical data (see Fig. 4) have been averaged in both time and the homogeneous tangential direction.

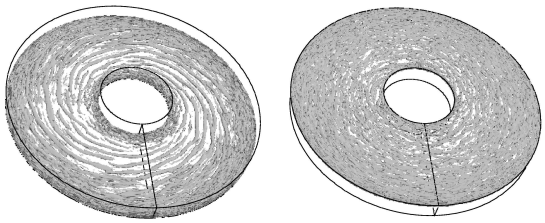

Figure 3: LES results showing coherent structures of the flow at $Re = 4 \times 10^5$. Iso-surface of the Q-criterium ($Q = 0.03$). Transitional turbulent rotor (left) layer with large spiral arms in the middle, characteristics of the unstable laminar flow. Turbulent stator (right) layer with much finer and axisymmetric structures than in the rotor.

The agreement between measurements and computations is satisfying at $Re = 4 \times 10^5$. The mean flow (Fig. 4a) is broadly a Batchelor flow as in the laminar regime, with two boundary layers separated by a core in solid body rotation. Indeed, on average, there exists a main flow in the tangential direction coupled with a secondary flow in the $(r,\, z)$ plane. The differences in the thickness and shape of the radial velocity profile near the two discs suggest that the level of turbulence is higher in the stator layer than in the rotor layer as expected at this Reynolds number. The LES computations predicts a mean velocity in the core, $V = 0.363r$ in very good agreement with experimental measurements $V = 0.353r$. The main Reynolds-stress components have been accurately computed and confirm the presence of a

fully turbulent stator layer and a still laminar rotor layer at mid-radius. An examination of the off-diagonal Reynolds stresses from LES results shows that these normal stresses are dominant. The two profiles (Fig. 4b) show a satisfying agreement between numeric and experiment. Let's notice however, that the agreement between the maxima in stator layer is less satisfying, with a LES value smaller (respectively larger) in the radial direction (respectively in the tangential direction) than the experimental measurement. As a consequence, the anisotropy of the normal stresses is stronger in LES than in experiment. As would be inferred from a stress budget, the normal stress is greatest in the tangential direction, exceeding by a factor of about 2 those in the two other directions. However, this anisotropy is shown to decrease when the turbulence level increases. The location of the normal stresses maxima is relatively well predicted within the stator layer for both radial and tangential directions; at a distance from the stator equal to $0.05h$ for the radial component and two times closer $0.025h$ for the tangential component.

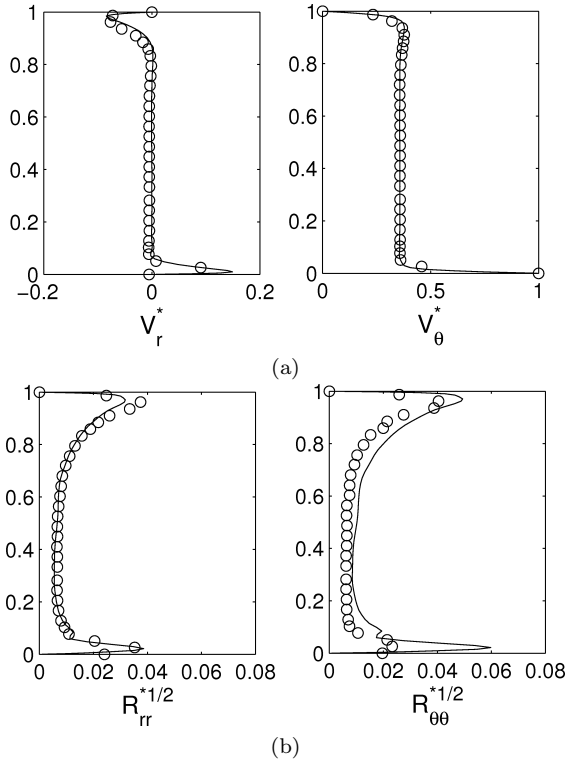

Figure 4: Numerical (Black triangles) and experimental (white circles) statistical data at mid- radius and $Re = 4 \times 10^5$. All the quanti-ties have been normalized by the local velocity of the rotor $\Omega.r$. The stator is located at $z = 1$ and the rotor at $z = 0$. (a) Mean velocity of radial and tangential components, respectively. (b) Square root of the two first diagonal components of the Reynolds stress tensor $\overline{V_r'^2}$ and $\overline{V_\theta'^2}$.

$Re = 10^6$

The flow regime is now fully turbulent both in the stator and rotor layers. SVV computation has been carried out on the grid $(N_1, N_2, N_3) = (121, 250, 81)$ with a time step $\delta t = 5 \times 10^{-5}\Omega^{-1}$. The SVV parameters have been chosen equal to $(\epsilon_1, \epsilon_2, \epsilon_3) = (\frac{1}{2.N_1}, \frac{1}{N_2}, \frac{1}{2.N_3})$ and $(\omega_{T_1}, \omega_{T_2}, \omega_{T_3}) = (\sqrt{\omega_{c_1}}, \sqrt{\omega_{c_2}}, \sqrt{\omega_{c_3}})$. The statistical data (see Fig. 5) are still averaged in both time and the homogeneous tangential direction. The agreement between measurements and computations at $Re = 10^6$ are satisfying even if less accurate to predict the averaged data than at $Re = 4 \times 10^5$.

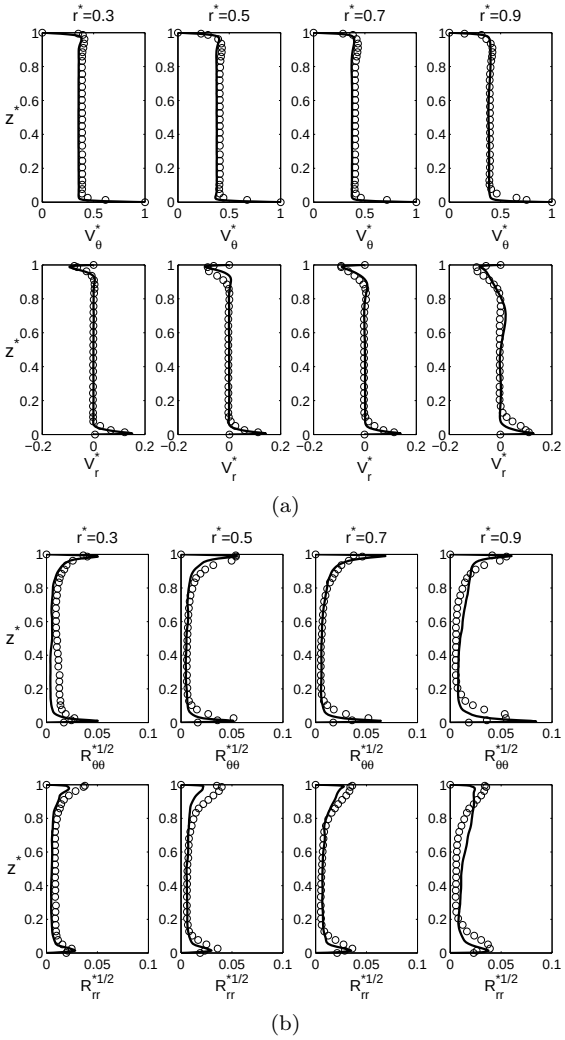

Figure 5: Numerical (Black triangles) and experimental (white circles) statistical data at mid-radius and $Re = 10^6$. All the quantities have been normalized by the local velocity of the rotor $\Omega.r$. The stator is located at $z = 1$ and the rotor at $z = 0$. (a) Mean velocity of radial and tangential components, respectively. (b) Square root of the two first normal components of the Reynolds stress tensor $\overline{V_r'^2}$ and $\overline{V_\theta'^2}$.

The differences in the thickness and shape of the measured main Reynolds-stress components profile near the two discs suggest that the level of turbulence is equal in the rotor layer and in the stator layer as expected at this Reynolds number. The LES computations predicts a mean velocity in the core, $V = 0.378r$ in very good agreement (8.11% smaller) with experimental measurements $V = 0.409r$. While the LES computations predict a level of turbulence 23.85% higher in the stator than in experiment and a level of turbulence 5.80% smaller in the rotor than in the experiment (see Fig. 5b). However we have a very satisfying level of turbulence within the core region, and an excellent estimation of the position of the turbulence peaks, respectively at $0.013h$ for both stresses in the stator and at $0.026h$ in the rotor for

the experiment and $0.018h$ for the computation. Those results at $Re = 10^6$ explain while most eddy-viscosity models fail to capture a correct solution.

Indeed, most eddy viscosity models are based on some assumptions on the turbulent boundary layers. More precisely they use either the hypothesis of isotropy or of homogeneity in one direction. But it's neither the case here. Although the turbulence statistics and structures are similar for three dimensional and two dimensional boundary layers (3DTBL and 2DTBL respectively), there is some major differences including the magnitude and angle of the shear stress vector in the layer. Near a wall, we can consider the shear stress vector in each plane parallel to the wall and study the gap, δ_γ, between its angle, γ_τ, and the angle of the mean gradient vector, γ_g (displayed in Fig. 6); and we can study its magnitude relative to the turbulence magnitude, measured by the Townsend structural parameter: $a_1 = \tau/(2k)$ (displayed in Fig. 7).

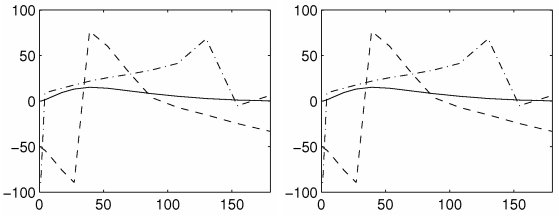

Figure 6: Axial evolutions of the three characteristic angles in wall units for $Re = 10^6$ at $r^* = 0.5$ along the rotor side (left) and along the stator side (right). (—) γ_m, (- -) γ_g, (-.-) γ_τ.

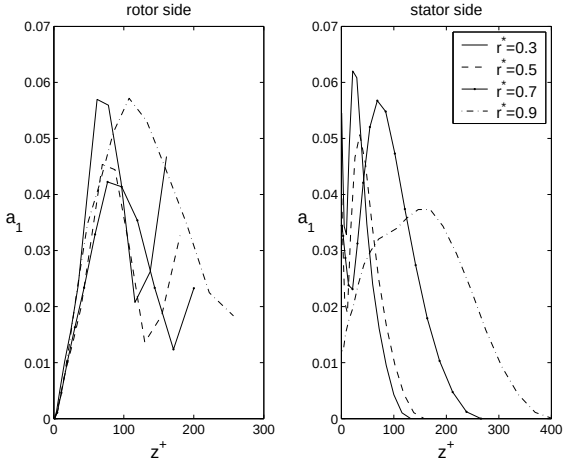

Figure 7: Townsend structural parameter $a_1 = \tau/(2k)$ on both disk at different radius for $Re = 10^6$.

One characteristics of the three-dimensional turbulent boundary layer is the reduction of the Townsend structural parameter $a_1 = \tau/(2k)$, defined as the ratio of the shear stress vector magnitude τ to twice the turbulent kinetic energy k. We have reported in figure 9 the variation at four radial locations of a_1 in wall units z^+ in both boundary layers. We can see clearly a significant reduction below the limiting value 0.15 for a two-dimensional turbulent boundary layer, with behaviors similar to those reported by Itoh et al. (1995) and Littell and Eaton (1994) from their measurements. It suggests the three-dimensional turbulent nature of the flow along the rotor and stator walls. This reduction of a_1 indicates also that the shear stress in this type of flow is less efficient in extracting turbulence energy from the mean field. Note that $a_1 > 0.15$ is obtained only very locally on the inner and outer cylinders.

To fix the three-dimensional nature of the boundary layers, we display in figure 6 the axial variations of the three characteristic angles in wall coordinates z^+: the mean velocity angle $\gamma_m = arctan(V_r/V_\theta)$, the mean gradient velocity angle $\gamma_g = arctan(\frac{\partial V_r}{\partial z}/\frac{\partial V_\theta}{\partial z})$ and the turbulent shear stress angle $\gamma_\tau = arctan(\overline{V_r'.V_z'}/\overline{V_\theta'.V_z'})$. The profile of γ_m clearly shows the continuous change of direction of the mean velocity vector with the distance from the wall, one of the major characteristics of three-dimensional turbulent boundary layer. The angle remains in the range $-1^o < \gamma_m < 17^o$ within the Ekman layer and in the range $-34^o < \gamma_m < 1^o$ within the Bödewadt layer. Another feature of 3DTBL is that the direction of the Reynolds shear stress vector in planes parallel with the wall is not aligned with the mean velocity gradient vector. Such a misalignment is observed in the present LES on both disks. The lag between γ_τ and γ_g is large towards the boundary layers with a maximum value about 100^o on the rotor to be compared with the value 18^o reported by Lygren and Andersson (2004) in infinite disk system. In their numerical study of non-stationary 3DTBL, Coleman et al. (2000) obtained large values of the lag especially near the wall and inferred it from the slow growth of the spanwise component of the shear stress. These authors observed also the change of the sign of the gradient angle γ_g. Such large values of this lag make the assumption of eddy-viscosity isotropy to fail for the prediction of such flows. In the present case, this feature indicates a strong three-dimensionality with highly distorted flow field resulting from the shear induced by rotation over the disks, adding another complexity in comparison with the idealized configuration in Lygren and Andersson (2004).

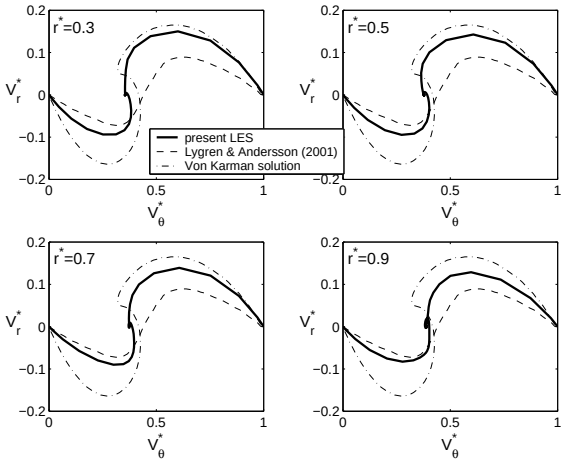

Figure 8: Polar plot of the velocity distribution in the whole gap between the two disks at $Re = 10^6$ for different radius. Comparison between (—) LES results, (-.-) laminar Von Karman solution, and (- -) DNS results of Lygren and Andersson (2004).

Some may observe that our Townsend structural parameters are closer to the 3BTBL than those of Lygren and Andersson (2004) while our polar plot (see Fig. 8) is closer to the laminar case. This behaviour may be explained by the presence of shrouds in our cavity that add more perturbation to the boundary layers since we have multiple impacts of different strength and different nature and can generate all but more anisotropy in the layers. On the other hand, those ending walls breaks the flow on the disk region near

the cylinders and thus it frees less space for the flow to aim at the case of Lygren and Andersson with infinite radial extension.

CONCLUSION

The authors conduct here a parallel investigation both experimentally and numerically of shrouded rotor-stator flow at high Reynolds number up to 10^6. The highly accurate computation of turbulent rotating flows within cavity is of interest for both engineering applications with turbomachinaries, and fundamental research, as one of the simplest cases where the turbulent boundary layers should be three-dimensional. Such flows are difficult to compute when using spectrally accurate numerical schemes, this result directly from the fact that spectral approximations are much less diffusive than low order ones. Nevertheless the numerical approach is of Large Eddy Simulation using a 3D spectral code stabilized with a Spectral Vanishing Viscosity model, which is, at our knowledge, the first LES result of such kind of flow providing highly accurate data. Statistical results agree favorably both with experiments and with previous alternative works found in the literature. Moreover the authors confirmed that the boundary layers are fully 3D on both the rotor and the stator, which explains the inaptitude of eddy-viscosity models that use isotropy or homogeneity assumptions to provide accurate results on this domain of Reynolds number.

ACKNOWLEDGEMENT

The authors acknowledge the IDRIS (CNRS)computing centre where the computations were performed on the Nec SX5 supercomputer (program 060242). The authors are very grateful to Professors R. Pasquetti (CNRS / Lab. J. Dieudonné Nice) and B.E. Launder (Univ. of Manchester) for fruitful discussions. The work was supported by CNRS in the frame of the DFG-CNRS program "LES of complex flows". Support for E. Séverac by a CNRS grant is also acknowledged.

REFERENCES

H.I. Andersson and M. Lygren. LES of open rotor-stator flow. *Int. J. Heat Fluid Flow*, 27(4):551–557, 2006.

G.N. Coleman, J. Kim, P.R. Spalart. A numerical study of strained three-dimensional wall-bounded turbulence. *J. Fluid Mech.*, 416:75–116, 2000.

J.W. Daily and R.E. Nece. Chamber dimension effects on induced flow and frictional resistance of enclosed rotating disks. *ASME J. Basic Eng.*, 82:217–232, 1960.

M. Itoh. Experiments on the turbulent flow in the narrow clearance between a rotating and a stationary disk. Ed. B.F. Carroll, T. Kobayashi and M.J. Morris, *Turbulent flows*, ASME-FED, vol.208, pages 27–32, 1995.

G.S. Karamanos and G.E. Karniadakis. A spectral vanishing viscosity method for large eddy simulation. *J. Comp. Phys.*, 163:22–50, 2000.

H.S. Littell and J.K. Eaton. Turbulence characteristics of the boundary layer on a rotating disk. *J. Fluid. Mech.*, 266:175–207, 1994.

J.L. Lumley. Computational modeling of turbulent flows. *Adv. Appl. Mech.*, 18:123–176, 1978.

M. Lygren and H.I. Andersson. Turbulent flow between a rotating and a stationary disk. *J. Fluid. Mech.*, 426:297–326, 2001.

M. Lygren and H.I. Andersson. Large eddy simulations of the turbulent flow between a rotating and a stationary disk. *Z. Angew. Math. Phys.*, 55:268–281, 2004.

R. Pasquetti and C.J. Xu. High-order algorithms for large-eddy simulation of incompressible flows. *J. Sci. Comp.*, 17(1-4):273–284, 2002.

S. Poncet, M.P. Chauve, and P. Le Gal. Turbulent rotating disk with inward throughflow. *J. Fluid. Mech.*, 522:253–262, 2005.

S. Poncet, M.P. Chauve, and R. Schiestel. Batchelor versus stewartson flow structures in a rotor-stator cavity with throughflow. *Phys. Fluids*, 17(7), 2005.

A. Randriamampianina and S. Poncet. Turbulence characteristics of the Bödewadt layer in a large enclosed rotor-stator system. *Phys. Fluids*, 18: 055104, 2006.

I. Raspo, S. Hugues, E. Serre, A. Randriamampianina, and P. Bontoux. A spectral projection method for the simulation of complex three-dimensional rotating flows. *Computers and Fluids*, 31:745–767, 2002.

L. Schouveiler, P. Le Gal and M.P. Chauve. Instabilities of the flow between a rotating and a stationary disk. *J. Fluid Mech.*, 443:329-350, 2001.

E. Serre, P. Bontoux and B.E. Launder. Direct Numerical Simulation of transitional turbulent flow in an enclosed rotor-stator cavity. *Flow, Turbulence & Combustion*, 69:35–50, 2002.

E. Serre, E. Crespo del Arco and P. Bontoux. Annular and spiral patterns in flows between rotating and stationary discs. *J. Fluid Mech.*, 434:65–100, 2001.

E. Séverac, E. Serre, R. Pasquetti and B.E. Launder, A stabilization technique to study turbulent rotating flows using high-order numerical method, *In Advances in Turbulence X*, 861, CIMNE, Eds. H.I. Andersson, P.A. Krogstad, Barcelona 2004.

E. Séverac and E. Serre. A spectral vanishing viscosity LES model for the simulation of turbulent flows within rotating cavities. *submitted to J. Comp. Phys.*, 2006.

E. Tadmor. Convergence of spectral methods for nonlinear conservation laws. *SIAM J. Numer. Anal.*, 26(1):30–44, 1989.

X. Wu and K.D. Squires. Prediction and investigation of the turbulent flow over a rotating disk. *J. Fluid. Mech.*, 418:231–264, 2000.